Evolution of rarefaction pulses into vortex rings

Natalia G. Berloff*
Department of Mathematics, University of California, Los Angeles, California 90095-1555
(Received 2 October 2001; revised manuscript received 25 February 2002; published 29 April 2002)

The two-dimensional solitary waves of the Gross-Pitaevskii equation in the Kadomtsev-Petviashvili limit are unstable with respect to three-dimensional perturbations. We elucidate the stages in the evolution of such solutions subject to perturbations perpendicular to the direction of motion. Depending on the energy (momentum) and the wavelength of the perturbation different types of three-dimensional solutions emerge. In particular, we present new periodic solutions having very small energy and momentum per period. These solutions also become unstable and this secondary instability leads to vortex ring nucleation.

DOI: 10.1103/PhysRevB.65.174518 PACS number(s): 67.40.Vs, 02.60.Cb, 05.45.−a, 67.55.Fa

I. INTRODUCTION

The recent achievements of Bose-Einstein condensation (BEC) in trapped alkali-metal gases[1] has stimulated a tremendous interest in the dynamics of BEC. From the first BEC experiments attempts were made to create trapped quantized vortices and successes in this direction have led to an intense theoretical activity in study of vortices, their structure, energy, and stability.[2] Over the years many different methods for the creation of vortices in trapped BEC's were suggested and implemented. Recently vortex rings were generated in two-component BEC by the decay of dark solitons through the snake instability.[3] This method was motivated by the observed decay of optical dark solitons into point vortices through a similar mechanism.[4]

The classical field description of the strongly degenerate weakly interacting Bose gas is given by the Gross-Pitaevskii (GP) equation.[5] At low temperatures the GP model gives a precise description of the atomic condensates and their dynamics. The same equation has been the subject of extensive studies also in the framework of superfluid helium at very low temperature, although in this case the GP model gives only a qualitative description of superfluid helium. In this paper we consider different mechanisms that create vortex rings from irrotational solitary solutions of the GP model. We are also interested in determining the entire solitary-wave sequences of solutions of the GP model because they define possible states that can be excited in a Bose condensate.

Jones and Roberts[6] determined the entire sequence of axisymmetric solitary solutions numerically for the GP model:

$$-2i\psi_t=\nabla^2\psi+(1-|\psi|^2)\psi, \tag{1}$$

where we use dimensionless variables such that the unit of length corresponds to the healing length a, the speed of sound is $c=1/\sqrt{2}$, and the density at infinity is $\rho_\infty=1$. The axisymmetric solitary-wave solutions satisfy two conditions: (1) the disturbance associated with the wave vanishes at large distances, $\psi\to 1$, $|\mathbf{x}|\to\infty$, and (2) they preserve their form as they propagate with a dimensionless velocity U, so that $\psi(x,y,z,t)=\psi(x',y,z)$, $x'=x-Ut$, in three dimensions (3D) and $\psi(x,y,t)=\psi(x',y)$, in two dimensions (2D), so that the solitary-wave solutions satisfy

$$2iU\frac{\partial\psi}{\partial x'}=\nabla^2\psi+(1-|\psi|^2)\psi. \tag{2}$$

Jones and Roberts calculated the energy $\mathcal{E}$ and momentum $\mathcal{P}$ given by

$$\mathcal{E}=\frac{1}{2}\int|\nabla\psi|^2dV+\frac{1}{4}\int(1-|\psi|^2)^2dV, \tag{3}$$

$$\mathcal{P}=\frac{1}{2i}\int[(\psi^*-1)\nabla\psi-(\psi-1)\nabla\psi^*]dV, \tag{4}$$

and determined the location of the sequence on the $\mathcal{P}\mathcal{E}$ plane.

In three dimensions they found two branches meeting at a cusp where $\mathcal{P}$ and $\mathcal{E}$ assume their minimum values $\mathcal{P}_{\min}$ and $\mathcal{E}_{\min}$. As $\mathcal{P}\to\infty$ on each branch, $\mathcal{E}\to\infty$. On the lower branch the solutions are asymptotic to large vortex rings.

As $\mathcal{E}$ and $\mathcal{P}$ decrease from infinity along the lower branch, the solutions begin to lose their similarity to large vortex rings. Eventually, for a momentum $\mathcal{P}_0$ slightly greater than $\mathcal{P}_{\min}$, they lose their vorticity (ψ loses its zero), and thereafter the solitary solutions may better be described as "rarefaction waves." The upper branch consists entirely of these and, as $\mathcal{P}\to\infty$ on this branch, the solutions asymptotically approach the rational soliton solution of the Kadomtsev-Petviashvili type-I (KPI) equation[7] and are unstable. In 2D the family of the solitary-wave solutions is represented by two point vortices if $U\leqslant 0.4$. As the velocity increases the wave loses its vorticity and becomes a rarefaction pulse. As $U\to 1/\sqrt{2}$ both the energy $\mathcal{E}$ and momentum $\mathcal{P}$ per unit length approach zero and the solutions asymptotically approach the 2D rational soliton solution of the KPI equation.

Jones and Roberts[6] derived the KPI equation using an asymptotic expansion in the parameter $\epsilon^2\approx 2(1-\sqrt{2}U)$, which is small when U approaches the speed of sound. They sought solutions of the form $\psi=f+ig$, where $f=1+\epsilon^2 f_1+\epsilon^4 f_2+\cdots$, $g=\epsilon g_1+\epsilon^3 g_2+\cdots$, and $U=1/\sqrt{2}+\epsilon^2 U_1+\cdots$. The independent variables were stretched, so that $\xi=\epsilon x'$, $\eta=\epsilon^2 y$, and $\zeta=\epsilon^2 z$. By substituting these expressions into Eq. (2) and considering real and imaginary parts at the leading and first orders in ϵ, they determined that g_1 satisfies the KPI equation

$$\frac{\partial^2 g_1}{\partial \xi^2}+\nabla^2_{\eta\zeta} g_1-\frac{\partial}{\partial \xi}\left[\frac{1}{2}\frac{\partial^3 g_1}{\partial \xi^3}-\frac{3}{\sqrt{2}}\left(\frac{\partial g_1}{\partial \xi}\right)^2\right]=0, \qquad (5)$$

and $f_1=\partial g_1/\sqrt{2}\partial\xi-g_1^2$, $U_1=-1/2\sqrt{2}$. In 2D, Eq. (5) has a closed-form solution,[8] so that the asymptotic solution of the GP equation in the KPI limit is

$$\psi=1-i\frac{2\sqrt{2}x'}{x'^2+\epsilon^2y^2+3/2\epsilon^2}-\frac{2}{x'^2+\epsilon^2y^2+3/2\epsilon^2}, \qquad (6)$$

which we have written in the original variables.

It was shown by Kuznetsov and Turytsin[9] that the 2D KPI soliton is stable to 2D but unstable to 3D perturbations. A linear stability analysis of the 2D solitary solution of the GP equation subject to long-wavelength infinitesimal perturbations was done by Kuznetsov and Rasmussen.[10] They demonstrated that all long-wavelength antisymmetric modes are stable and all long-wave length symmetric modes are unstable. In particular they showed that the growth rates of symmetric perturbations, σ, is given by $\sigma^2=-\mathcal{E}k^2/(\partial\mathcal{P}/\partial U)>0$, as the wave number $k\to 0$. The maximum growth rates of instability and the instability region of 2D solitary solutions were found by Berloff and Roberts[11] by solving the linear stability problem. Through numerical integration of the GP equation it was shown that as perturbations grow to finite amplitude the vortex lines reconnect to produce a sequence of almost circular vortex rings. Senatorski and Infeld[12] numerically integrated the KPI equation to study the fate of 2D KPI solitons subject to 3D perturbations. They determined that 2D KPI solitons evolve into 3D KPI solitons which are also unstable.

The goal of this paper is to elucidate the fate of the 2D rarefaction pulse in the KPI limit of the GP model subject to 3D perturbations. We discovered that such solutions may evolve into vortex rings and this establishes a new mechanism of vortex nucleation. We found that this mechanism can operate in different ways. The intermediate states may involve periodic solutions consisting of interacting 3D rarefaction pulses that belong to the lower branch of the Jones-Roberts cusp with $\mathcal{P}<\mathcal{P}_0$.

II. NUCLEATION OF VORTEX RINGS

We have performed direct numerical simulations using the numerical method described in Ref. 13 We solve the GP equation in the reference frame moving with the velocity U_f chosen in such a way that the main disturbance is kept within the computational box:

$$-2i\frac{\partial\psi}{\partial t}+2iU_f\frac{\partial\psi}{\partial x'}=\nabla^2\psi+(1-|\psi|^2)\psi. \qquad (7)$$

In these computations we follow the evolution of the asymptotic solution (6) extended along the z axis and moving in the x direction. The dimensions of the computational box are $D_x=60$, $D_y=60$, and $D_z=180$. The xy faces of the box are open to allow sound waves to escape; this is achieved numerically by applying the Raymond-Kuo technique.[14] The $z=0$ and $z=D_z$ sides are reflective.

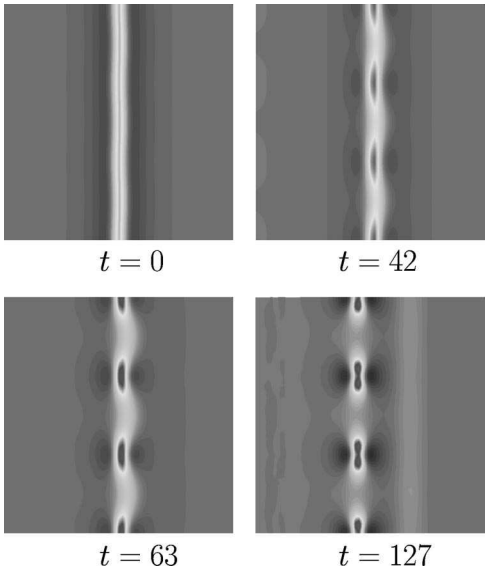

FIG. 1. The contour plot of the density field of the cross section of solutions of the GP equation. The time snapshots show the evolution of the KPI solution (6) of the GP equation in the xz plane with $y=D_y/2$. In Eq. (6) we took $\epsilon=0.5$ and the wavelength of the initial perturbation (8) is $l=20$. The solutions starting with the third panel possess vorticity and evolve into equally spaced vortex rings.

The soliton (6) was perturbed along the z axis, so that at $t=0$

$$x'\to x'+0.1\cos(kz). \qquad (8)$$

We choose k so that N periods of this perturbation fit exactly into the D_z dimension of the box. There are two main parameters of the problem that determine the final outcome of the instability: ϵ, which determines the configuration, energy, and momentum of the initial field, and the wavelength of the perturbation, $l=D_z/N$. It can be easily shown using Eq. (6) that the energy (3) and the momentum (4) of our initial field per wavelength of perturbation are given by

$$\mathcal{E}=\mathcal{P}/\sqrt{2}=8\pi\epsilon l/3. \qquad (9)$$

First, we consider the evolution of the KPI solitary solution subject to large wavelength perturbations $l=20,30,60$ and $\epsilon=0.5$. Figure 1 illustrates the appearance of vortex rings through contour plots of the cross section of the solution in the xz plane with $y=D_y/2$ for $l=20$.

According to the time snapshots of Fig. 1 the solution evolves directly into a set of vortex rings; other axisymmetric 3D solutions including 3D KPI solitons are not involved. Moreover, exactly one vortex ring is generated for each wavelength of the perturbation. These vortex rings are distanced l healing lengths apart and have radii much smaller than l (see Table I). They therefore interact only weakly with each other. The energy and momentum (9) of one period of the perturbation are used to create one vortex ring; the extra energy and momentum escape and are carried away by transients, including sound waves (phonons). The vortex rings

TABLE I. The energy and momentum per wavelength of the perturbation of the initial field; the energy, momentum, velocity, and radius of the resulting vortex ring, and the amount of energy and momentum lost as the percentage of the initial energy and momentum.

l	$\mathcal{E}_{\text{init}}$	$\mathcal{P}_{\text{init}}$	$\mathcal{E}_{\text{ring}}$	$\mathcal{P}_{\text{ring}}$	U_{ring}	R_{ring}	$\%\mathcal{E}$ lost	$\%\mathcal{P}$ lost
60	251	355	99	162	0.45	2.7	60	54
30	126	178	86	132	0.49	2.35	32	26
20	84	120	71	102	0.53	1.9	15.5	15

are aligned and propagate together with the same velocity. This arrangement of vortex rings is itself unstable and cannot last forever.

Similar calculations were done for $l=30$ and $l=60$. The results are summarized in Table I which gives the energy and momentum per wavelength of the perturbation of the initial field; the energy, momentum, velocity, and radius of the resulting vortex ring; and the amount of energy and momentum lost as the percentage of the initial energy and momentum.

From Table I we can see that the extra energy, $\Delta\mathcal{E}=\mathcal{E}_{\text{init}}-\mathcal{E}_{\text{ring}}$, and momentum, $\Delta\mathcal{P}=\mathcal{P}_{\text{init}}-\mathcal{P}_{\text{ring}}$, for lower wavelengths are carried away by exclusively sound waves since $\Delta\mathcal{E}\approx c\Delta\mathcal{P}$. We can also calculate the critical value of the wavelength, l_{crit}, for creation of vortex rings. The Jones-Roberts solitary solutions lose their vorticity at $\mathcal{E}_0\approx 56$, $\mathcal{P}_0\approx 78.5$, and $R_0\approx 1$.[6] The wavelength of the perturbation of the initial field, l_{crit}, that leads to the nucleation of the vortex of such minimal energy and radius can be found from the expression

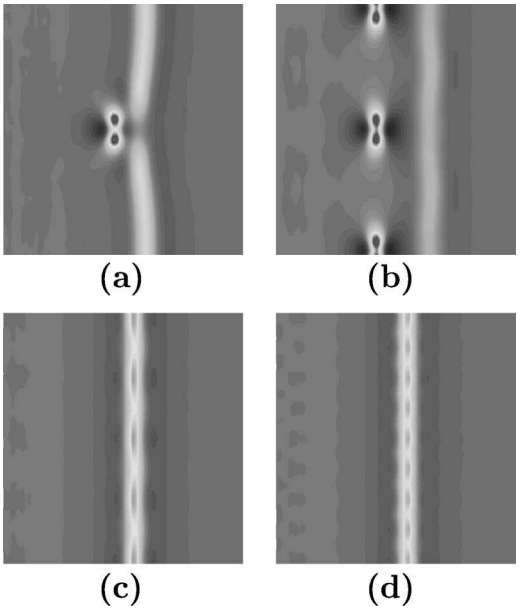

FIG. 2. The contour plot of the density field of the cross-section of solutions of the GP equation. The time snapshots show the different stages in the evolution of the KPI limit solution (6) of the GP equation in the xz plane with $y=D_y/2$. In Eq. (6) we took $\epsilon=0.5$ and the wavelengths of the initial perturbation (8) were $l=60$ (a), $l=30$ (b), $l=15$ (c), and $l=7.5$ (d). The contour plots are shown for $|\psi|^2$ at $t=149$ for (a) and $t=127$ for the rest of panels.

TABLE II. The energy and momentum of the initial field and the resulting periodic rarefaction solution.

l	$\mathcal{E}_{\text{init}}$	$\mathcal{P}_{\text{init}}$	$\mathcal{E}_{\text{per}}$	$\mathcal{P}_{\text{per}}$
15	62	90	55	78
7.5	31.5	46.2	30.7	44
3.75	15.5	23	15	21

$$\mathcal{E}_{\text{init}}=\mathcal{E}_{\text{sound}}+\mathcal{E}_0. \tag{10}$$

Our numerical calculations indicate that the minimal energy loss to sound waves during the transition to vortex rings is approximately 15%, so the energy carried away by sound waves is $\mathcal{E}_{\text{sound}}\approx 0.15\mathcal{E}_{\text{init}}$ with $\mathcal{E}_{\text{init}}$ given by Eq. (9). Therefore, from Eq. (10)

$$l_{\text{crit}}\approx 7.86/\epsilon. \tag{11}$$

This result agrees very well with our numerical calculations for $\epsilon=0.5$, which give $l_{\text{crit}}\approx 16$.

III. PERIODIC RAREFACTION PULSE

Next we explore the evolution of the KPI limit solitary waves of the GP model subject to perturbations with wavelength $l<l_{\text{crit}}$. The effect of the decrease in the wavelength of the perturbation is twofold: (1) the energy and the momentum (9) per wavelength of the initial field are decreased, therefore leaving less energy available for creating a new entity, and (2) these entities are in close proximity to each other so they strongly interact. Figure 2 plots the cross sections of the solutions for $\epsilon=0.5$ and $l=60,30,15,7.5,3.75$. The first two panels [Figs. 2(a) and 2(b)] illustrate the vortex nucleation discussed earlier. To the best of our knowledge the periodic solutions shown on Figs. 2(c)–2(e) are unknown in the literature on the GP model or the nonlinear Schrödinger equation. The interesting feature of these solutions is that they lack a vorticity and have small energy and momentum per period that tend to zero as $l\to 0$. These solutions can be understood as periodic pulse trains composed of rarefaction pulses positioned on the lower branch of the Jones-Roberts sequence with $\mathcal{P}<\mathcal{P}_0$. These periodic solutions can execute standing-wave oscillations of decreasing amplitude

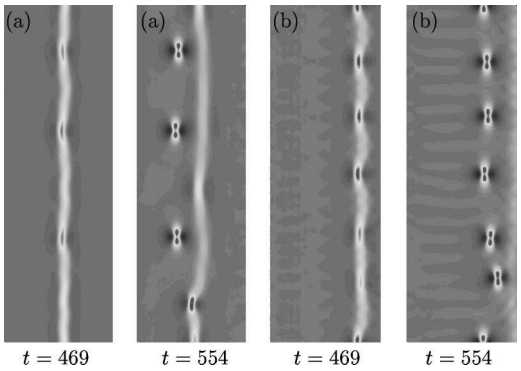

FIG. 3. The contour plot of the density field of the cross section of solutions of the GP equation. The time snapshots show the different stages in the evolution of the KPI limit solution (6) of the GP equation with $\epsilon=0.5$ in the xz plane with $y=D_y/2$. The wavelengths of the initial perturbation (8) are $l=15$ (a) and $l=7.5$ (b).

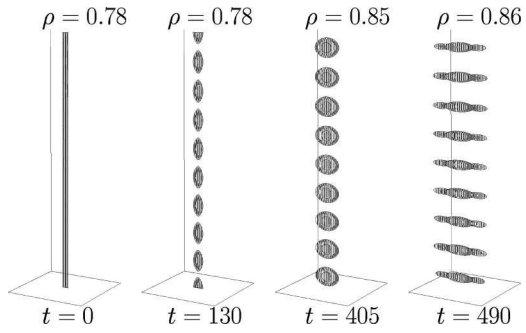

FIG. 4. Isosurfaces of the density field of solutions of the GP equation. The time snapshots show the different stages in the evolution of the KPI limit solution (6) of the GP equation with $\epsilon = 0.3$. The wavelength of the initial perturbation (8) is $l = 15$. The minimum density increases with time and approaches unity as the solution breaks down into sound waves.

and period $l/2$. The interaction between adjacent pulses reduces the total energy per period. The analysis of these and other properties of periodic pulse trains composed from the solitary waves of nonintegrable evolution equations can be found in Ref. 15.

Other findings are summarized in Table II which gives the values of the energy and momentum of the initial field and the resulting periodic rarefaction solution.

For the Korteweg–de Vries equation and some other integrable equations Whitham[16] demonstrated that an infinite linear superposition of the solitons in a periodic pulse train is also a solution. This result generally is not true for nonintegrable systems. Berloff and Howard[15] introduced a method of constructing a periodic pulse train solution of nonintegrable equations as an infinite superposition of *modified* solitary waves. Note that these methods were developed for solitons exponentially decaying at infinity. The energy per period of a periodic pulse train is greatly reduced as compared with the energy of the solitary wave it is made of. The solitary-wave solutions of the GP equation decay as rational functions at infinity:

$$\mathrm{Re}\,\psi \sim 1 + mU(3x'^2 - s^2)s^{-5}, \tag{12}$$

$$\mathrm{Im}\,\psi \sim -mx's^{-3}, \tag{13}$$

where m is the dipole moment and $s^2 = x'^2 + (1-2U^2)(y^2 + z^2)$. Therefore, the effect of the solitary wave interactions is even more pronounced for the GP periodic solutions. We can compare the energy and momentum of the solution with the period $l = 3.75$ (the last entry of Table II) with the energy, $\mathcal{E} = 51$, and momentum, $\mathcal{P} = 70$, of the rarefaction solitary pulse. The interactions reduced the energy and momentum by 70%.

Similarly to the periodic solutions made of aligned vortex rings, the periodic rarefaction solutions become unstable and we followed the development of this instability. Figure 3(a) shows the contour plots of the density for a cross section of the field which evolves from the periodic rarefaction solution with $l = 15$ to produce a total of four rings. Therefore, to create each ring the energy and momentum of several periods of the rarefaction solution were used. The wavelength of the secondary instability that destroyed the periodic solution is approximately 57. Similar calculations were done for the even shorter perturbation wavelength $l = 7.5$; see Fig. 3(b). The wavelength of the secondary instability is approximately 29, resulting in the appearance of six rings. The reason for the apparent nonuniformity of the nucleated rings is that D_z is not an exact multiple of these wavelengths.

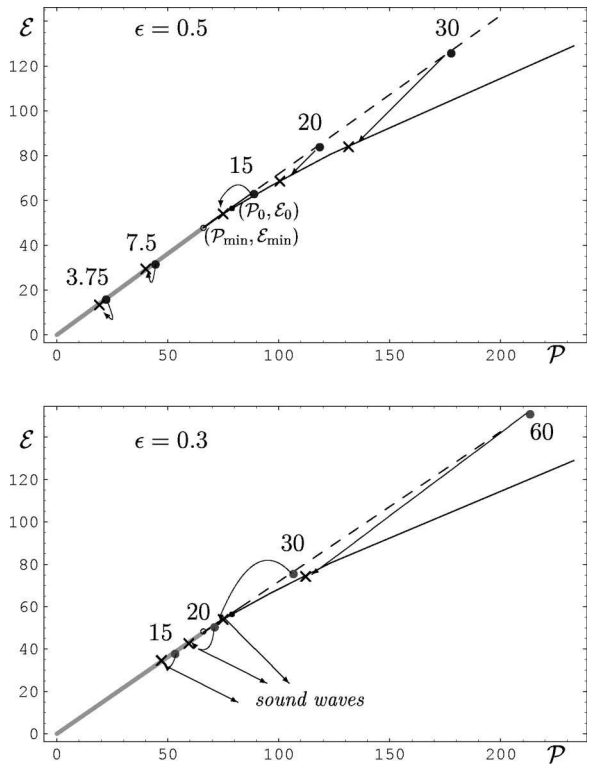

FIG. 5. Summary of the numerical integration of Eq. (7) starting with the initial condition (6) with $\epsilon = 0.5$ and $\epsilon = 0.3$. The cusp corresponds to the 3D solitary-wave solutions. The upper branch is shown by dashes to indicate that this branch is unstable. $(\mathcal{P}_0, \mathcal{E}_0)$ marks the point where the vorticity disappears and point $(\mathcal{P}_{\min}, \mathcal{E}_{\min})$ gives the position of the lowest momentum-energy state of the 3D solitary solution (see discussion in the text). The line from the origin to $(\mathcal{P}_{\min}, \mathcal{E}_{\min})$ corresponds to the family of periodic rarefaction pulses. Dots indicate the position of the initial states, and the wavelength of the perturbation l is given next to each initial state; arrows show the evolution of these solutions, and the crosses correspond to the final state before the onset of the secondary instability.

IV. SOUND-WAVE GENERATION

Finally, we consider the evolution of the small energy and momentum KPI limit solitary waves. In these computations we use $\epsilon = 0.3$ and $l = 60, 30, 20, 15$. For $l = 60$ the KPI solution follows the scenario of vortex nucleation and directly evolves into three vortex rings of small radii. For smaller wavelengths $l = 30, 20, 15$ the KPI solution initially evolves into oscillating periodic rarefaction pulses of decreasing y extent. The energy and momentum per period are apparently insufficient to allow them to evolve into rings and the necessary energy cannot be reduced through interactions when

the putative solutions are separated by such large distances. These solutions break down into sound waves that carry off all energy and momentum; see Fig. 4.

V. CONCLUSIONS

In summary, we studied the instability of the 2D KPI limit solitary wave solution in the GP equation. The evolution of several types of solutions is considered. We were able to identify three different regimes of transition depending on the initial energy and momentum of the KPI solution and on the wavelength of the initial perturbation. For large wavelengths, the initial solution immediately evolves into a periodic solution consisting of small equally spaced vortex rings with a period equal to the period of the initial perturbation. For shorter wavelengths the KPI solution first evolves into a periodic solution consisting of 3D interacting rarefaction pulses that later break up into vortex rings under the influence of a secondary instability of a different wavelength. Finally, if the energy of the KPI solution is small, the solution can break into sound waves after forming an oscillating periodic rarefaction pulse.

Figure 5 summarizes all calculations performed and the relationships of the different regimes studied. The initial states considered are represented by dots on the $\mathcal{PE}$ plane, where $\mathcal{E}$ and $\mathcal{P}$ are defined per wavelength of the perturbation. We plot the cusp determined by Jones and Roberts[6] for the family of the vortex rings and rarefaction pulses. The arrows show the way the initial state evolves.

ACKNOWLEDGMENTS

This work was supported by the NSF Grant Nos. DMS-9803480 and DMS-0104288. It arose from the suggestion by Dr. Sergey Nazarenko to elucidate the instability of rarefaction pulses. I am very grateful to Professor Paul Roberts for many useful discussions about this work.

*Electronic address: nberloff@math.ucla.edu

[1] M. H. Anderson *et al.,* Science **269**, 198 (1995); K. B. Davis *et al.,* Phys. Rev. Lett. **75**, 3969 (1995); C. C. Bradley *et al.*, *ibid.* **78**, 985 (1997).

[2] A. L. Fetter and A. A. Svidzinsky, J. Phys.: Condens. Matter **13**, R135 (2001).

[3] B. P. Anderson, P. C. Haljan, C. A. Regal, D. L. Feder, L. A. Collins, C. W. Clark, and E. A. Cornell, Phys. Rev. Lett. **86**, 2926 (2001).

[4] A. V. Mamaev, M. Saffman, and A. A. Zozulya, Phys. Rev. Lett. **76**, 2262 (1996).

[5] V. L. Ginzburg and L. P. Pitaevskii, Zh. Éksp.Teor. Fiz. **34**, 1240 (1958) [Sov. Phys. JETP **7**, 858 (1958)]; E. P. Gross, Nuovo Cimento **20**, 454 (1961); L. P. Pitaevskii, Sov. Phys. JETP **13**, 451 (1961).

[6] C. A. Jones and P. H. Roberts, J. Phys. A **15**, 2599 (1982).

[7] B. B. Kadomtsev and V. I. Petviashvili, Sov. Phys. Dokl. **15**, 39 (1970).

[8] S. V. Manakov, V. E. Zakharov, L. A. Bordag, A. R. Its, and V. B. Matveev, Phys. Lett. **63A**, 205 (1977).

[9] E. A. Kuznetsov and S. K. Turytsin, Sov. Phys. JETP **55**, 844 (1982).

[10] E. A. Kuznetsov and J. Juul Rasmussen, Phys. Rev. E **51**, 4479 (1995).

[11] N. G. Berloff and P. H. Roberts, J. Phys. A **34**, 10057 (2001).

[12] A. Senatorski and E. Infeld, Phys. Rev. E **57**, 6050 (1998).

[13] N. G. Berloff and P. H. Roberts, J. Phys. A **33**, 4025 (2000).

[14] G. W. Raymond and H. L. Kuo, Q. J. R. Meteorol. Soc. **110**, 525 (1984).

[15] N. G. Berloff and L. N. Howard, Stud. Appl. Math. **99**, 1 (1997); **100**, 195 (1998).

[16] G. B. Witham, IMA J. Appl. Math. **32**, 353 (1984).